Appl. Phys. A 67, 371–378 (1998)

Applied Physics A
Materials
Science & Processing

Optical characterization of thermally evaporated thin films of $As_{40}S_{40}Se_{20}$ chalcogenide glass by reflectance measurements

E. Márquez[1,*], J.M. González-Leal[1], R. Prieto-Alcón[1], M. Vlcek[2], A. Stronski[3], T. Wagner[2], D. Minkov[4]

[1] Departamento de Física de la Materia Condensada, Facultad de Ciencias, Universidad de Cádiz, 11510 Puerto Real, Cádiz, Spain
[2] Department of General and Inorganic Chemistry, Faculty of Chemical Technology, University of Pardubice, 53210 Pardubice, Czech Republic
[3] Institute of Semiconductor Physics, Ukrainian Academy of Sciences, Department of Photochemical Phenomena in Semiconductors, 252028 Kiev, Ukraine
[4] Research Institute for Fracture Technology, Tohoku University, Sendai, Japan

Received: 11 February 1998/Accepted: 16 February 1998

Abstract. Optical reflection spectra, at normal incidence, of ternary chalcogenide thin films of chemical composition $As_{40}S_{40}Se_{20}$, deposited by thermal evaporation, were obtained in the 400 nm to 2200 nm spectral region. The optical constants of this amorphous material were computed using an optical characterization method based mainly on the ideas of Minkov and Swanepoel of utilising the upper and lower envelopes of the spectrum, which allows us to obtain both the real and imaginary parts of the complex refractive index, and the film thickness. Thickness measurements made by a surface-profiling stylus have been carried out to cross-check the results obtained by the optical method. The dispersion of the refractive index is discussed in terms of the single-oscillator Wemple–DiDomenico model. The optical band gap has been determined from absorption coefficient data by Tauc's procedure. Finally, the photo-induced and thermally induced changes in the optical properties of a-$As_{40}S_{40}Se_{20}$ thin films were also studied, using both transmission and reflection spectra.

PACS: 78.20.Ci; 78.66.Jg

Optical properties of chalcogenide glasses, such as excellent transmittance in the infrared region, continuous shift of the optical-absorption edge, and values of refractive index ranging between around 2.0 and 3.5, as well as very strong correlation between the former properties and the chemical composition, explain the significant interest in these amorphous materials for the manufacture of filters, antireflection coatings and, in general, a wide range of optical devices [1–4]. Furthermore, the broad range of photo-induced effects that the chalcogenide glasses exhibit (such as photocrystallization, photo-polymerization, photo-decomposition, photo-vaporization, photo-dissolution of certain metals, and photo-vitrification [5, 6]), generally accompanied by large changes in the optical constants [7, 8] and, particularly, shifts in the absorption edge (i.e., photo-darkening or photobleaching), is also interesting for technological applications. This underlines the importance of the characterization of these glassy materials by accurate determination of their optical constants, refractive index, and extinction coefficient, as well as the corresponding optical band gap.

Existing methods for determining the optical constants of thin films, are usually based on sophisticated computer iteration techniques [9–12], using both optical transmission and reflection spectra, or only the transmission spectrum. A relatively simple method for computation of the optical constants, using only the optical reflection spectrum, at normal incidence, is employed in this work (mainly based on ideas (Minkov and Swanepoel) of using the upper and lower envelopes of the spectrum [13–15]). These two envelopes are computer drawn according to a useful algorithm developed by McClain et al. [16]. An important advantage of this optical method is that, when the reflection spectrum is utilised rather than the transmission spectrum, a greater number of interference extrema (or, equivalently, tangent points) occur, which leads to reduced errors when calculating the film thickness and the refractive index [13]. In this paper, this method is used to calculate accurately the optical constants and the thickness of uniform thermally evaporated thin films of the ternary glassy composition $As_{40}S_{40}Se_{20}$. The fact that there is a lack of literature data concerning optical characterization of thin films of ternary chalcogenide glasses highlights the significance of the present study. In addition, the changes of the optical constants induced by thermal annealing and light exposure are also briefly described.

1 Experimental details

The bulk glass was prepared according to the conventional melt-quenched method. The elements were weighted and

* Corresponding author.
Fax: +34-56/834924, E-mail: marquez@galeon.uca.es

placed in a precleaned and outgassed quartz ampoule, which was evacuated to a pressure of about 10^{-3} Pa and then sealed. The synthesis was performed in a rocking furnace at $\approx 715\,^{\circ}$C for about 6 h. Then, the ampoule was quenched in water at a temperature of $\approx 15\,^{\circ}$C, which is equivalent to a cooling rate of the order of $10\,\mathrm{K\,s^{-1}}$. Next, the thin-film samples were prepared by vacuum evaporation of the powdered melt-quenched glassy material onto clean glass substrates (microscope slides). The thermal evaporation process was performed within a coating system (Tesla Corporation, model UP-858) at a pressure of about 10^{-4} Pa. During the deposition process the substrates were conveniently rotated by means of a planetary rotation system, which makes it possible to obtain as-deposited glass films of outstanding uniform thickness. The deposition rate was ≈ 6–$8\,\mathrm{nm\,s^{-1}}$, measured by the dynamical weighting method. This deposition rate results in a film chemical composition that is very close, indeed, to that of the bulk starting material. The composition of the chalcogenide films was found to be $As_{39.8\pm0.5}S_{39.9\pm0.6}Se_{20.3\pm0.3}$ on the basis of the electron microprobe X-ray analysis (Jeol, model JSM-820). The lack of crystallinity in the films was verified by X-ray diffraction (XRD) measurements (Philips, model PW-1820); a typical XRD pattern is displayed in Fig. 1. The thickness of the a-$As_{40}S_{40}Se_{20}$ films studied ranged between around 0.8 μm and 1.4 μm. The mass densities of the specimens were derived from the weighting of them (Mettler, model AE200), before and after deposition of the layer [17].

Regarding the structure of the films, attention should be drawn to the so-called first sharp diffraction peak (FSDP) or pre-peak in the structure factor, $S(Q)$ [18, 19] (see Fig. 1). This peak almost invariably occurs at a value of the scattering vector $Q \approx 1\,\mathrm{Å^{-1}}$ in amorphous chalcogenides (in the present case, at a value of Q of approximately $1.1\,\mathrm{Å^{-1}}$). This feature is referred to as a pre-peak because Fourier transformation of $S(Q)$, both including and omitting this peak, produces essentially indistinguishable real-space correlation functions, indicating that the peak does not contain structural information about the short-range order, being associated instead with subtle medium-range order structural arrangements.

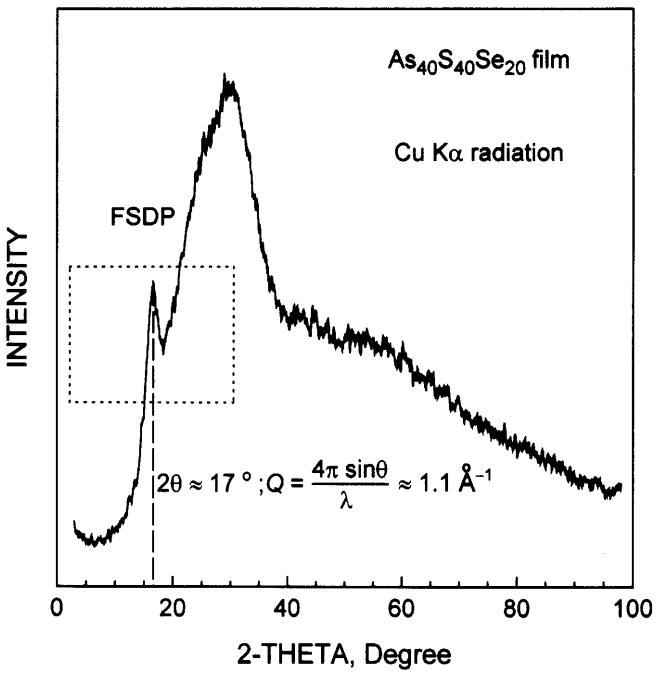

Fig. 1. Typical XRD pattern (Cu K_α radiation) corresponding to a representative $As_{40}S_{40}Se_{20}$ thin film deposited on a glass substrate (the data have been smoothed by means of the Savitzky–Golay filter)

The reflection spectra were obtained by a double-beam ratio recording UV/Vis/NIR spectrophotometer, with automatic computer data acquisition (Perkin-Elmer, model Lambda-l9), and the wavelength range analyzed was between 400 nm and 2200 nm. The reflection measurements were carried out against a very accurately calibrated front-surface aluminium mirror coated with magnesium fluoride, which was taken as a reference. Since the absolute reflectance of the calibrated mirror is known, the relative reflectance of the thin-film sample, obtained by means of the spectrophotometer, can be converted to absolute reflectance. On the other hand, the reflection measurements were made in various parts of the glass films, scanning the entire sample, and a very good reproduction of the reflection spectrum was generally achieved. The spectrophotometer was set with a slit width of 1 nm. A surface-profiling stylus (Sloan, model Dektak 3030) was also used to measure independently the film thickness, which was compared with the thickness calculated from the reflection spectrum. All optical measurements reported were performed at room temperature.

2 Preliminary theoretical considerations

The optical system under consideration is a homogeneous film with a constant thickness d and a complex refractive index $n_c = n - \mathrm{i}\,k$, where n is the refractive index and k the extinction coefficient, which can be expressed in terms of the absorption coefficient α by the equation: $k = \alpha\lambda/4\pi$. The thickness of the substrate is several orders of magnitude larger than d and its refractive index is designated by s. Interference effects in the thin film give rise to reflectance curves similar to those in Fig. 2a, which shows an optical reflection spectrum of a representative $As_{40}S_{40}Se_{20}$ chalcogenide film. The interference fringes are used to calculate accurately the optical constants and the thickness of the glass films. At a wavelength λ of the studied spectral region, the reflectance $R(\lambda, s, n, d, k)$ of the optical system mentioned earlier, is a complex function ((3) from [13]). It is known that for weakly absorbing dielectric films, when the conditions $n \gg k$ and $s \gg k$ are met in the spectral region considered, this equation is dominated by the exponential terms in the optical absorbance ($x = \exp(-\alpha d)$) and the contribution of k in the other terms of the expression becomes negligibly small, and k can be considered to be zero [13, 20]. This simplifies notably the expression for the reflectance, which becomes a function of n and x only. Expressions for the top and bottom envelopes of the reflection spectrum, R_M and R_m, are given by (5) from [13], for $k = 0$ and dielectric films with $n > s \gg k$. The top envelope, R_M, lies above the spectrum, i.e., $R_M \geq R(\lambda)$, whereas the bottom envelope, R_m, lies below the spectrum, i.e., $R_m \leq R(\lambda)$. It should be pointed out that, in the present work, the refractive index of the substrate s is calculated independently from the reflection spectrum of the

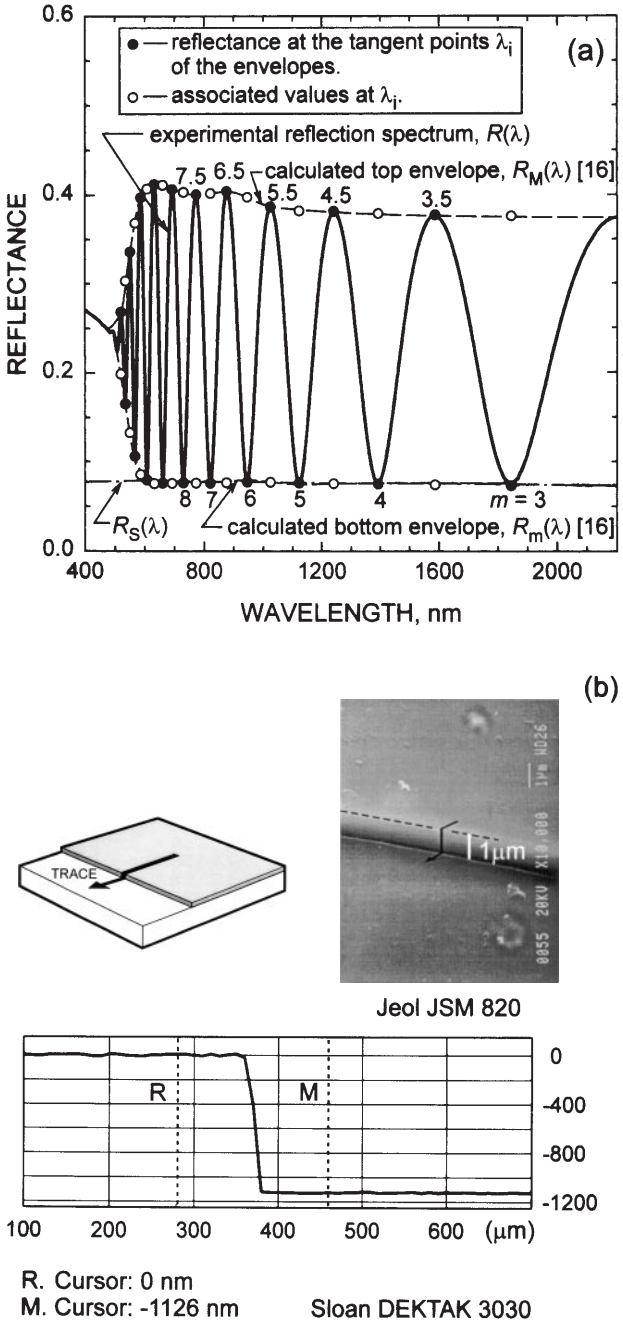

Fig. 2. a Experimental reflection spectrum of the representative $As_{40}S_{40}Se_{20}$ thin film. The order number m is a half-integer for the tangent points of the higher envelope, $R_M(\lambda)$, and an integer for the tangent points of the lower envelope, $R_m(\lambda)$. R_S is the bare substrate reflection. **b** The record obtained by use of a surface-profiling stylus and, also, a scanning electron microscope (SEM) micrograph of a thin-film sample

bare substrate, R_S, by the relationship

$$R_S = \frac{(s-1)^2}{s^2+1}\,, \tag{1}$$

from which is derived

$$s = \frac{1+\sqrt{R_S(2-R_S)}}{1-R_S}\,. \tag{2}$$

3 Results and discussion

3.1 Calculation of the refractive index and the film thickness

First of all, it is necessary to draw the envelopes R_M and R_m, illustrated in Fig. 2a. As already mentioned, these envelopes are very carefully drawn using the computer program created by McClain et al. Their work gives an accurate method for calculation of the two envelopes of a given set of oscillatory data, based on determination of the corresponding tangent points between the set of data and the envelopes. The main steps for calculation of envelopes are: (i) smoothing of the data, (ii) estimation of the locations of the upper and lower tangent points and, (iii) interpolation of a cubic spline through the estimated upper tangent points and another through the estimated lower tangent points. Due to the specific behaviour of the reflection spectrum in the spectral region of medium absorption, it is not possible to use a simple parabolic interpolation when drawing the two envelopes of reflection spectra, nevertheless such interpolation is acceptable for transmission spectra [15]. It is found that the tangent points coincide with the maxima and minima of the reflection spectrum in the transparent region, but not in the medium and strong absorption region. The presence of absorption in the film leads to smaller wavelengths for the tangent points λ_i, with respect to the corresponding extremum points λ_{extr} (i.e., $\lambda_i \leq \lambda_{extr}$). The effect of absorption is corrected by using the values of R and its envelopes at the tangent points, instead of the extremum points of the spectrum [21].

Once the tangent points λ_i between the two envelopes and the reflection spectrum are known, and the refractive index of the substrate s is calculated from the reflection spectrum of the bare substrate, R_s, the system of two transcendental equations corresponding to (5) from [13], is solved numerically using the Newton–Raphson method. A distinct advantage of using the envelopes of the reflection spectrum rather than only the reflection spectrum, is that the envelopes are slow-changing functions of λ, whereas the spectrum varies rapidly with λ. Correspondingly, the above-mentioned system of two equations with two unknowns has only one solution for n and x. Therefore, n and x are determined for all of the tangent points λ_i associated with the upper and lower envelopes, created by the McClain et al.'s algorithm, as solutions of the systems

$$\begin{aligned} R_M(\lambda_i) - R_M(n_i, x_i) &= 0\,, \\ R_m(\lambda_i) - R_m(n_i, x_i) &= 0\,, \end{aligned} \tag{3}$$

where $R_M(\lambda_i)$ and $R_m(\lambda_i)$ are "experimental" values of the two envelopes at the tangent point λ_i. For each tangent point, the solution of this system provides an initial approximation for the refractive index and absorbance of the thin film studied, n_i^0 and x_i^0, respectively, and these values are listed in Table 1.

The algorithm for calculation of the final spectral dependences $n(\lambda)$ and $k(\lambda)$, and the film thickness of a thin layer, using only the reflection spectrum, is explained in [13]. The calculations are performed in the same sequence as in the method proposed by Swanepoel [15], where the transmission spectrum is used. In order to calculate the initial approximation for the film thickness, it is necessary to take into account the well-known equation for the interference fringes, which,

Table 1. Values of λ, s, R_M, and R_m corresponding to the optical reflection spectrum of Fig. 2a. Calculation of the thickness and the refractive index based on the present optical method

λ/nm	s	R_M	R_m	n^0	x^0	d^0/nm	m^0	m	d^1/nm	n^1
1845	1.483	0.376	0.073	2.437	1.000	—	3.36	3.0	1136	2.417
1587	1.489	0.377	0.074	2.444	1.000	1161	3.92	3.5	1136	2.426
1393	1.492	0.379	0.075	2.453	1.000	1162	4.48	4.0	1136	2.433
1241	1.494	0.382	0.076	2.462	1.000	1155	5.04	4.5	1134	2.439
1123	1.497	0.382	0.076	2.466	1.000	1197	5.58	5.0	1138	2.452
1025	1.500	0.387	0.077	2.484	1.000	1182	6.16	5.5	1135	2.462
946	1.501	0.398	0.077	2.522	1.000	1217	6.78	6.0	1125	2.479
876	1.498	0.404	0.076	2.543	1.000	1164	7.38	6.5	1119	2.486
821	1.496	0.402	0.076	2.534	1.000	1290	7.85	7.0	1134	2.510
773	1.496	0.401	0.076	2.530	1.000	1307	8.32	7.5	1146	2.532
730	1.497	0.403	0.076	2.539	1.000	1292	8.84	8.0	1150	2.550
692	1.495	0.406	0.076	2.548	1.000	1304	9.36	8.5	1154	2.569
660	1.496	0.411	0.076	2.567	1.000	1390	9.89	9.0	1157	2.594
632	1.494	0.412	0.075	2.567	1.000	1451	10.30	9.5	1169	2.622
607	1.511	0.410	0.079	2.519	1.000	1523	10.50	10.0	1205	2.651

$\overline{d^0} = 1271\,\text{nm} \pm 117\,\text{nm}$ (9.2%); $\overline{d^1} = 1145\,\text{nm} \pm 21\,\text{nm}$ (1.8%)

because of absorption, is verified at the tangent points

$$2nd = m\lambda\,, \tag{4}$$

where the order number m is an integer for a minimum and a half-integer for a maximum. Moreover, if n_i and n_{i+1} are the refractive indices for two adjacent tangent points with wavelengths λ_i and λ_{i+1}, respectively, the expression for the approximate thickness at each tangent point is

$$d = \frac{\lambda_i \lambda_{i+1}}{4(\lambda_i n_{i+1} - \lambda_{i+1} n_i)}\,. \tag{5}$$

The values of d determined by this equation are listed as d^0 in Table 1. The average of the values of d determined by this equation, $\overline{d^0}$, is a first estimation of the film thickness. The $\overline{d^0}$ value corresponding to the representative $As_{40}S_{40}Se_{20}$ film is $1271\,\text{nm} \pm 117\,\text{nm}$ (9.2%). This value is used, together with the values of n^0, to calculate the "order number", m^0, using (4) for the different tangent points. The accuracy of the film thickness is then significantly increased by taking the corresponding exact integer or half-integer values of m, associated with each tangent point (see Fig. 2a), and deriving a new thickness, d^1, from (4), again using the n^0 values. The values of m^0, m, and d^1 are also presented in Table 1. The new values for the thickness do have a much smaller dispersion and its average value is taken as the final thickness of the film. The average thickness for the representative film is $1145\,\text{nm} \pm 21\,\text{nm}$ (1.8%). In addition, the film thickness determined by mechanical measurements on the same film area was $1126\,\text{nm} \pm 22\,\text{nm}$ (see Fig. 2b, where a SEM micrograph of a specimen is also shown), in excellent agreement, indeed, with the thickness obtained by the optical method – the difference being less than 2%.

Additionally, a simple, complementary graphical method proposed by Swanepoel [15], for deriving independently the values of the first order number m_1 and the film thickness, based on (4), is also used. This expression is rewritten for that purpose as

$$\frac{\ell}{2} = 2d\frac{n}{\lambda} - m_1\,, \tag{6}$$

where $\ell = 0, 1, 2, \ldots$. Therefore, plotting $\ell/2$ against n/λ gives a straight line with slope $2d$ and a cut-off on the y axis of $-m_1$. Figure 3 displays this graph for the representative sample, while the values obtained for d and m_1 are 1197 nm and 3.27 (≈ 3), respectively. These values clearly confirm those previously calculated.

On the other hand, using the exact values of m and the $\overline{d^1}$ value, (4) is solved for n at each λ_i and, thus, the final values of the refractive index n^1 are obtained (these new values are also given in Table 1). The accuracy of the calculated values of the film thickness and the refractive index is limited by (i) the error of measurements of λ, which depends on the scale used, and for the case of Fig. 2a the maximum accuracy is about ± 1 nm or about 0.1%, and, (ii) on the other hand, by the maximum absolute accuracy of R_M and R_m, which is around

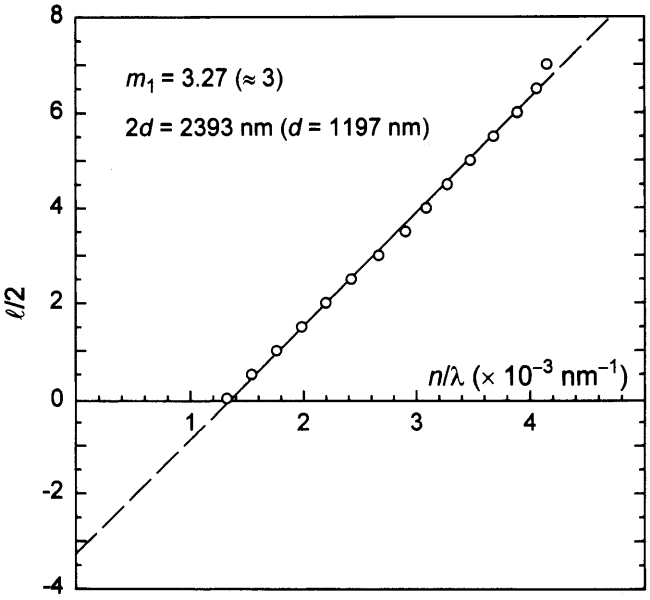

Fig. 3. Plot of $\ell/2$ against n/λ to calculate the first order number m_1 and film thickness d for the $As_{40}S_{40}Se_{20}$ thin-film sample

0.001 or around 0.5%. Moreover, it should be pointed out that the relative error in the calculated layer thickness is approximately equal to the relative error in the refractive index, i.e., $|\Delta d|/d \approx |\Delta n|/n$ (in the present case $< 2\%$).

The values of n^1 can be fitted to an appropriate function, such as the Wemple–DiDomenico dispersion relationship [22], i.e., to the single-oscillator model:

$$\varepsilon_1(\omega) = n^2(\omega) = 1 + \frac{E_0 E_\mathrm{d}}{E_0^2 - (\hbar\omega)^2}\,, \tag{7}$$

where $\hbar = h/2\pi$ (h is Planck's constant), ω is the frequency, $\varepsilon_1(\omega)$ is the real part of the complex electronic dielectric constant ($\varepsilon_\mathrm{c}(\omega) = \varepsilon_1(\omega) + \mathrm{i}\varepsilon_2(\omega)$), E_0 is the energy of the effective dispersion oscillator (typically near the mean peak of the $\varepsilon_2(\omega)$ spectrum), which is identified by the mean transition energy from the valence band of the lone-pair state to the conduction-band state (in these amorphous materials, the valence s states lie far below the top of the valence band, and the valence-band edge involves transitions between lone-pair p states and anti-bonding conduction-band states [22]), and E_d is the dispersion energy.

The oscillator energy, E_0 is an "average" energy gap and, in close approximation, it scales with the optical band gap, $E_\mathrm{g}^\mathrm{opt} : E_0 \approx 2 \times E_\mathrm{g}^\mathrm{opt}$, as was found by Tanaka [23]. The dispersion energy or oscillator strength, E_d, also follows a simple empirical relationship: $E_\mathrm{d} = \beta N_\mathrm{c} Z_\mathrm{a} N_\mathrm{e}$, where β is a constant, and according to Wemple [22], for "covalent" crystalline and amorphous materials has a value of 0.37 ± 0.04 eV. N_c is the coordination number of the "cations" surrounding an "anion", Z_a is the formal chemical valency of the anion, and N_e is the effective number of valence electrons per anion.

Plotting $(n^2-1)^{-1}$ against $(\hbar\omega)^2$ and fitting a straight line enables us to determine E_0 and E_d directly from the slope, $(E_0 E_\mathrm{d})^{-1}$, and the intercept on the vertical axis, E_0/E_d, respectively. The straight line equation corresponding to the least-squares fit is, $(n^2-1)^{-1} = 0.213 - 0.0108(\hbar\omega)^2$, with a correlation coefficient of 0.997 (see Fig. 4a). The values found for the Wemple–DiDomenico dispersion parameters E_0 and E_d, derived from the above-mentioned equation, are $E_0 = 4.44$ eV and $E_\mathrm{d} = 20.88$ eV. These values do seem to be rather consistent with those reported by Ramírez-Malo et al. [24] for $As_{40}S_{60}$ and $As_{40}Se_{60}$ binary chalcogenide glass films (these last values correspond to the stoichiometric compounds As_2S_3 and As_2Se_3 and were derived from optical transmission measurements only, making use one of the Swanepoel's methods for non-uniform thickness films [21]). In Table 2 are listed the obtained values of E_0, E_d, the value

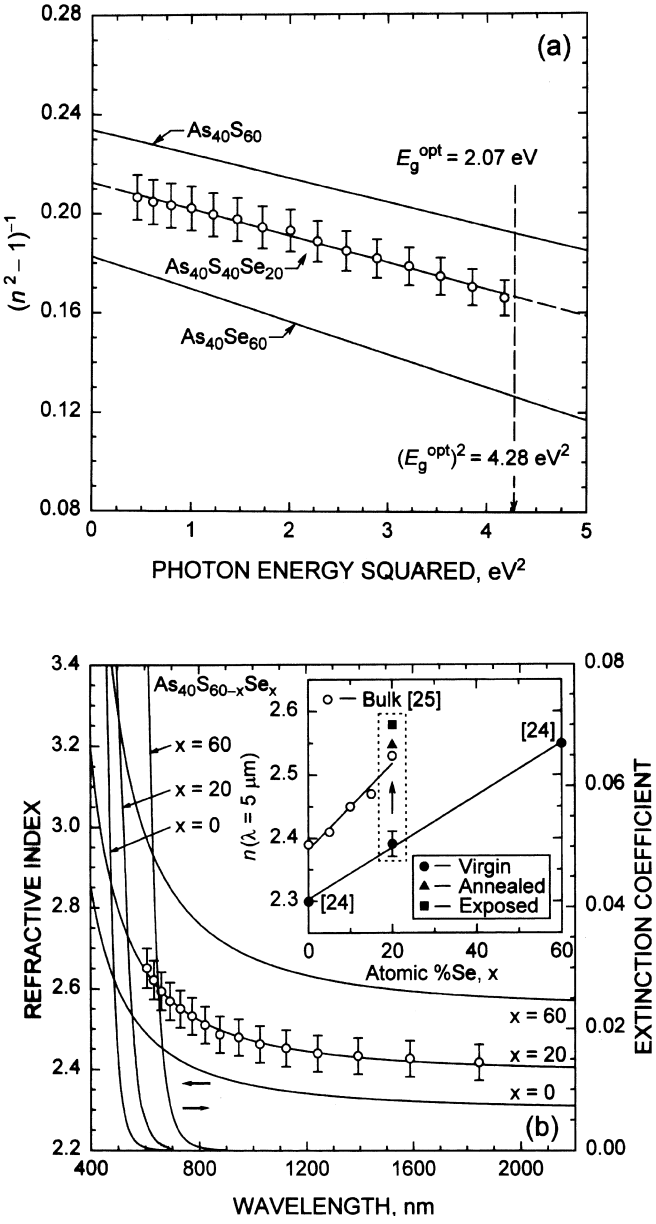

Fig. 4. a A plot of the factor $(n^2-1)^{-1}$ versus the photon energy squared $(\hbar\omega)^2$, for the representative $As_{40}S_{40}Se_{20}$ ternary thin film, in comparison with those of the $As_{40}S_{60}$ and $As_{40}Se_{60}$ binary thin films. **b** Refractive index n and extinction coefficient k versus wavelength for the three chalcogenide glassy compositions; the inset shows the refractive index at 5 μm versus Se content, for the As-S-Se bulk and thin-film samples (the values of n(5 μm) for the annealed and exposed $As_{40}S_{40}Se_{20}$ glass films are also plotted in the inset)

Table 2. Values of the single-oscillator energy or Wemple–DiDomenico "gap" (E_0), dispersion energy (E_d), refractive index at $\hbar\omega \to 0$ ($n(0)$), optical frequency dielectric constant (ε_∞), Tauc optical gap ($E_\mathrm{g}^\mathrm{opt}$), gap ratio ($E_0/E_\mathrm{g}^\mathrm{opt}$), Tauc slope ($B^{1/2}$), an alternative option for the optical gap (E_{04}), and the slope parameter of the Urbach region (E_e).

Composition	State	E_0/eV	E_d/eV	$n(0)$	ε_∞	$E_\mathrm{g}^\mathrm{opt}$/eV	$E_0/E_\mathrm{g}^\mathrm{opt}$	$B^{1/2}$/ $\mathrm{cm}^{-1/2}\,\mathrm{eV}^{-1/2}$	E_{04}/eV	E_e/meV
$As_{40}S_{60}$ [24]	Virgin	4.89	20.90	2.297	5.276	2.37	2.03	742	2.59	80
$As_{40}S_{40}Se_{20}$	Virgin	4.44 ± 0.03	20.88 ± 0.2	2.388 ± 0.001	5.703 ± 0.005	2.07 ± 0.01	2.14 ± 0.02	571 ± 5	2.34 ± 0.01	104 ± 1
$As_{40}S_{40}Se_{20}$	Annealed	4.36 ± 0.03	23.85 ± 0.2	2.544 ± 0.001	6.472 ± 0.005	2.04 ± 0.01	2.14 ± 0.03	647 ± 6	2.27 ± 0.01	123 ± 1
$As_{40}S_{40}Se_{20}$	Exposed	4.26 ± 0.04	23.99 ± 0.2	2.575 ± 0.002	6.631 ± 0.010	2.01 ± 0.02	2.12 ± 0.04	628 ± 8	2.25 ± 0.01	126 ± 1
$As_{40}Se_{60}$ [24]	Virgin	3.73	20.42	2.545	6.477	1.80	2.04	827	1.97	90

of the refractive index at $\hbar\omega \to 0$ (extrapolating the Wemple–DiDomenico optical dispersion equation towards the infrared spectral region), $n(0)$, and the optical frequency dielectric constant $\varepsilon_\infty (= n^2(0))$, for the three compositions. The value of $n(0)$ for the ternary composition $As_{40}S_{40}Se_{20}$, 2.388, is reasonably coherent with the $n(0)$ values for the binary compositions $As_{40}S_{60}$ and $As_{40}Se_{60}$. The Wemple–DiDomenico optical dispersion curves, as well as the corresponding linear fits, for these three glassy compositions under analysis, are shown in Fig. 4. Furthermore, it is stressed that the derivation of the film thickness and the refractive index of the as-deposited binary films has been carried out with a smaller number of tangent points in the transmission spectra, and a narrower spectral range studied, in the medium and weak absorption region, which leads to slight overvaluation of the refractive index and undervaluation of the average non-uniform film thickness.

The inset of Fig. 4b shows the change in the refractive index at $\lambda = 5\ \mu m$ versus Se content for $As_{40}S_{60-x}Se_x$ ternary bulk glasses, reported recently by Sanghera et al. [25]. The refractive index increases linearly with Se content, presumably due to the increased polarizability associated with the larger Se atom compared with S. Furthermore, a monotonic increase in molar refractivity has been found [25], which indicates that the addition of Se follows a simple additive law and there is no complex behaviour, which is in agreement with the proposed structure of these $As_{40}S_{60-x}Se_x$ bulk glasses, based on Raman spectroscopy [26]. The dependence of the refractive index at 5 μm on chemical composition, for the present as-deposited thin-film samples, is also plotted in the inset of Fig. 4b. These refractive indices also depend linearly on the Se content, but the value of the slope, 4.1×10^{-3}, is smaller than in the case of the compositional dependence of the bulk glasses, which is 6.8×10^{-3}.

The difference found between the values of the refractive index in the IR region of the $As_{40}S_{40}Se_{20}$ bulk glass and the corresponding virgin thin film, with the same ternary composition, is mostly due to a difference in their mass densities. The relationship between the refractive index, extrapolated towards the IR region, and the mass density, ρ, is given by the Lorentz–Lorenz equation [27]

$$\frac{\Delta n/n}{\Delta\rho/\rho} = \frac{\Delta n/n}{\Delta N/N} = \frac{(n^2-1)(n^2+2)}{6n^2}, \tag{8}$$

where N is the number of polarizable units per unit volume. The density of the virgin thin-film samples studied, $\approx 3.5\ g/cm^3$, and the density of the $As_{40}S_{40}Se_{20}$ bulk sample, $\approx 3.7\ g/cm^3$ [25], account fairly well for the difference between the calculated values of $n(5\ \mu m)(\approx n(0))$.

3.2 Derivation of the absorption and extinction coefficients and the optical band gap

The absorbance x is obtained by solving numerically either of the two expressions for the envelopes corresponding to (5) from [13]; it is possible to solve independently both equations for x, thereby obtaining two different values. In addition, since x and d are already known, the absorption and extinction coefficients can be determined. The results obtained from the envelope R_M are found to be superior, and this can be attributed to the fact that R_m is almost independent of n and k in the region of weak absorption where $x \approx 1$. Moreover, in the region of transparency, where $x = 1$, $R_m = R_s$, and it is seen from (1) that R_m is independent of n and k. Figure 5a shows the results obtained for α, and Fig. 4b those corresponding to k, using the upper envelope of the reflection spectrum.

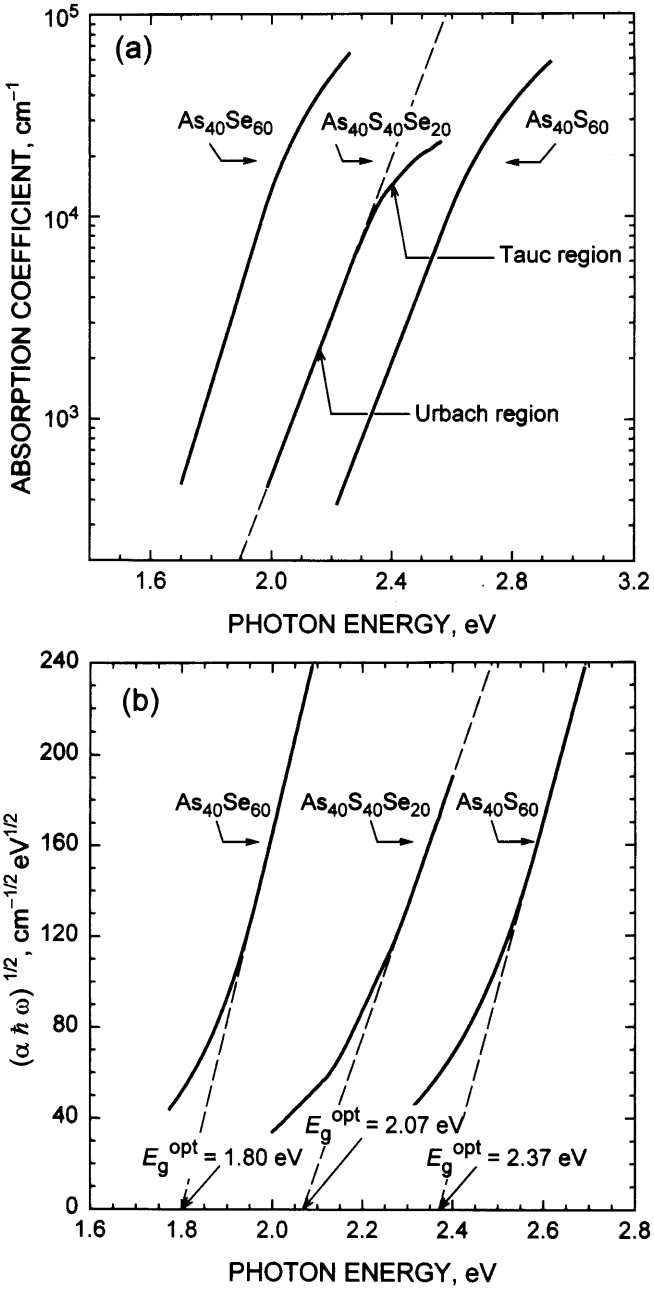

Fig. 5. a Absorption coefficient as a function of the photon energy for the three chalcogenide glassy compositions, $As_{40}S_{40}Se_{20}$ (this work), $As_{40}S_{60}$ and $As_{40}Se_{60}$. **b** Determination of the optical gap, E_g^{opt}, in terms of the Tauc law

It should be pointed out that the absorption coefficient of amorphous semiconductors, in the high-absorption region ($\alpha \gtrapprox 10^4\ cm^{-1}$), is given according to Tauc by the following equation [28]:

$$\alpha(\hbar\omega) = B\frac{(\hbar\omega - E_g^{opt})^2}{\hbar\omega}, \tag{9}$$

where E_g^{opt} and B are the optical gap and a constant, respectively. The dependence of α versus $\hbar\omega$ is displayed in Fig. 5a using a semi-logarithmic scale, for the representative $As_{40}S_{40}Se_{20}$ film, as well as for $As_{40}S_{60}$ and $As_{40}Se_{60}$ binary chalcogenide films. The Tauc gap is formally defined as the intersection of the straight line through the high-energy values of the graph of $(\alpha\hbar\omega)^{1/2}$ versus $\hbar\omega$, with the energy axis. Figure 5b shows such a plot for the above-mentioned films. Table 2 shows the values of the optical gap E_g^{opt} and the values of the slope parameter $B^{1/2}$, derived by Tauc's extrapolation, along with the values of the alternative optical gap, E_{04}, which represents the energy at which the absorption coefficient reaches the value of $10^4\,cm^{-1}$, for the considered chalcogenide films. It should be emphasized that the values of E_g^{opt} and E_{04} corresponding to the a-$As_{40}S_{40}Se_{20}$ film are very consistent with the values for the two other binary compositions.

Continuing with the analysis of the optical-absorption edge, at lower values of the absorption coefficient ($1\,cm^{-1} \lessapprox \alpha \lessapprox 10^4\,cm^{-1}$), the absorption depends exponentially on photon energy (the so-called Urbach relation [28])

$$\alpha(\hbar\omega) = \alpha_0 \exp\left(\frac{\hbar\omega}{E_e}\right), \qquad (10)$$

where E_e is a slope parameter (see Fig. 5a). The value of E_e found for the $As_{40}S_{40}Se_{20}$ film is ≈ 104 meV. The values of E_e for the $As_{40}S_{60}$ and $As_{40}Se_{60}$ films are also listed in Table 2.

3.3 Photo-induced and thermally induced darkening of amorphous $As_{40}S_{40}Se_{20}$ *films*

Some as-deposited a-$As_{40}S_{40}Se_{20}$ films were illuminated in air by a Hg arc lamp (through an IR-cut filter, providing broadband white light, with a very high UV output), with a light intensity of $\approx 40\,mW\,cm^{-2}$, during approximately 3 h (until reaching the saturation state). The effect of illumination was a clear redshift of their optical transmission spectra (see Fig. 6), i.e., a photo-darkening process has taken place in the glassy sample [29]. Similarly, after annealing at $\approx 160\,°C$ (the glass transition temperature, T_g, measured in a modulated differential scanning calorimetry experiment [30] was $\approx 199\,°C$, a value close to that reported by Sanghera et al. [25], $\approx 194\,°C$), for around 24 h, the as-deposited a-$As_{40}S_{40}Se_{20}$ film showed a thermal-darkening process (see also Fig. 6).

In addition, we have examined the refractive-index dispersion and the optical-absorption edge of the annealed and exposed glass films. For the accurate determination of the spectral dependence of the refractive index and the extinction coefficient we have used, as in the previous case of the virgin thin-film sample, the present procedure of the upper and lower envelopes of the reflection spectrum. In Table 2 are summarized the calculated values of $E_0, E_d, n(0)$, and ε_∞, belonging to the annealed and exposed samples; the values of the corresponding Tauc gaps, E_g^{opt}, together with the values of the gap ratio, E_0/E_g^{opt}, the Tauc slope, $B^{1/2}$, the optical gap, E_{04}, and, finally, the slope parameter of the Urbach region, E_e, are also listed in Table 2. From this particular table it follows that due to the annealing or the exposure of $As_{40}S_{40}Se_{20}$ glass film, the value of E_0 decreases, while the values of E_d, $n(0)$ and ε_∞ rather increase. On the other hand, the inset of Fig. 4b shows the values of the refractive index at 5 μm belonging to the annealed and exposed films. It is to be noted that the value of the refractive index corresponding to the annealed specimen is very close, indeed, to the value for the $As_{40}S_{40}Se_{20}$ bulk glass; the structure of the annealed films has usually been assumed to be similar to that of the corresponding bulk glasses [23]. Furthermore, it is evident from Table 2 the redshift of the Tauc gap, and the values of the gap ratio are practically more the same than in the case of virgin film, that is, $E_0/E_g^{opt} \approx 2$. The alternative option for the optical band gap, E_{04}, also decreases, and the values of parameters $B^{1/2}$ and E_e, clearly increase as a result of the thermal annealing or the light exposure. Additionally, the shifts of the short-wavelength edge (considering in this case the optical transmission spectra), ΔE, for the annealed and exposed films are shown in the inset of Fig. 6. A more detailed report on these particular experiments currently underway will be published elsewhere.

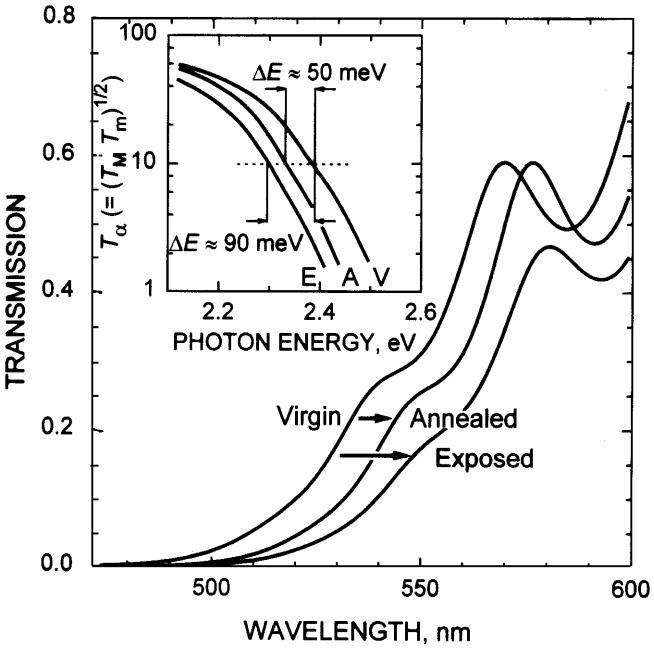

Fig. 6. Typical optical transmission spectra of the amorphous $As_{40}S_{40}Se_{20}$ film in the short-wavelength region. (V) Virgin, (A) annealed, and (E) exposed. The inset shows the spectral dependence of the smooth interference-free transmission curve, T_α, which is defined as the geometric mean of T_M and T_m [15]; the values of the shift of the short-wavelength edge, ΔE, for the cases of the thermal annealing and the light exposure, are also presented in the inset

4 Concluding remarks

An optical method for accurate calculation of both the film thickness and its optical constants, using only the reflection spectrum has been successfully applied to several uniform thermally evaporated $As_{40}S_{40}Se_{20}$ ternary chalcogenide films, with thicknesses ranging between around 0.8 μm and 1.4 μm. The almost perfect agreement between the reflectance of the lower envelope of the spectrum and the reflectance of the bare substrate, as well as the proof that the

error in the optical computation of the film thickness does not exceed 2%, are a clear indication for the high quality of the employed reflection measurement technique and for the large degree of planarity and homogeneity of the ternary chalcogenide thin films. The variation in thickness over the area of illumination, 1 mm × 10 mm, measured by the mechanical stepper, was found to be smaller than 10 nm.

Acknowledgements. The authors are grateful to Prof. R. Swanepoel (Rand Afrikaans University, Johannesburg, South Africa) and Dr. M. McClain (National Institute of Standards and Technology, Gaithersburg, USA) for some fruitful discussions. The use of the latest version (Envelope 2.01, 1997) of the computer program of Dr. McClain for drawing of envelopes is also acknowledged. Finally, the authors are also grateful to the anonymous referee for the enriching comments.

References

1. J.A. Savage: *Infrared Optical Materials and Their Antireflection Coatings* (Adam Hilger, Bristol 1985)
2. J. Tauc: *Amorphous and Liquid Semiconductors* (Plenum, New York 1974)
3. Z. Cimpl, F. Kosek: Phys. Status Solidi A **93**, K55 (1986)
4. D.A. Minkov, E. Vateva, E. Skordeva, D. Arsova, M. Nikiforova: J. Non-Cryst. Solids **90**, 481 (1987)
5. E. Márquez, R. Jiménez-Garay, A. Zakery, P.J.S. Ewen, A.E. Owen: Philos. Mag. B **63**, 1169 (1991)
6. E. Márquez, C. Corrales, J.B. Ramírez-Malo, J. Reyes, J. Fernández-Peña, P. Villares, R. Jiménez-Garay: Mater. Lett. **20**, 183 (1994)
7. E. Márquez, J.B. Ramírez-Malo, J. Fernández-Peña, P. Villares, R. Jiménez-Garay, P.J.S. Ewen, A.E. Owen: J. Non-Cryst. Solids **164**–**166**, 1223 (1993)
8. E. Márquez, J.B. Ramírez-Malo, J. Fernández-Peña, R. Jiménez-Garay, P.J.S. Ewen, A.E. Owen: Opt. Mater. **2**, 143 (1993)
9. J. Szcyrbrowski, A. Czapla: Thin Solid Films **46**, 127 (1977)
10. L. Vriens, W. Rippens: Appl. Opt. **22**, 4105 (1983)
11. D.P. Arndt, R.M.A. Azzam, J.M. Bennett, J.P. Borgogno, C.K. Carniglia, W.E. Case, J.A. Dobrowolski, U.J. Gibson, T. Tuttle Hart, F.C. Ho, V.A. Hodgkin, W.P. Klapp, H.A. Macleod, E. Pelletier, M.K. Purvis, D.M. Quinn, D.H. Strome, R. Swenson, P.A. Temple, T.F. Thonn: Appl. Opt. **23**, 3571 (1984)
12. D.A. Minkov: J. Mod. Opt. **37**, 1977 (1990)
13. D.A. Minkov: J. Phys. D: Appl. Phys. **22**, 1157 (1989)
14. J. Ruíz-Pérez, E. Márquez, D. Minkov, J. Reyes, J.B. Ramírez-Malo, P. Villares, R. Jiménez-Garay: Phys. Scr. **56**, 76 (1996)
15. R. Swanepoel: J. Phys. E: Sci. Instrum. **16**, 1214 (1983)
16. M. McClain, A. Feldman, D. Kahaner, X. Ying: J. Comput. Phys. **5**, 45 (1991)
17. W.A. Pliskin, S.J. Zanin: *Handbook of Thin Film Technology* (McGraw-Hill, New York 1983)
18. S.R. Elliott: Nature **354**, 445 (1991)
19. S.R. Elliott: Phys. Rev. Lett. **67**, 711 (1991)
20. R. Swanepoel: S. Afr. J. Phys. **12**, 148 (1989)
21. R. Swanepoel: J. Phys. E.: Sci. Instrum. **17**, 896 (1984)
22. S.H. Wemple: Phys. Rev. B **8**, 3767 (1973)
23. Ke. Tanaka: Thin Solid Films **66**, 271 (1980)
24. J.B. Ramírez-Malo, E. Márquez, C. Corrales, P. Villares, R. Jiménez-Garay: Mater. Sci. Eng., B **25**, 53 (1994)
25. J.S. Sanghera, V.Q. Nguyen, I.D. Aggarwal: J. Am. Ceram. Soc. **79**, 1324 (1996)
26. J. Freitas Jr., U. Strom, D.J. Treacy: J. Non-Cryst. Solids **59**&**60**, 875 (1983)
27. S. Rajagopalan, K.S. Harshavardhan, L.K. Malhotra, K.L. Chopra: J. Non-Cryst. Solids **50**, 29 (1982)
28. J. Tauc: J. Non-Cryst. Solids **8**–**10**, 569 (1972)
29. G. Pfeiffer, M.A. Paesler, S.C. Agarwal: J. Non-Cryst. Solids **130**, 111 (1991)
30. T. Wagner, S.O. Kasap: Philos. Mag. B **74**, 667 (1996)